

Mass of the black hole in the Seyfert 1.5 galaxy H 0507+164 from reverberation mapping

C. S. Stalin^{1*}, S. Jeyakumar², R. Coziol², R. S. Pawase³, S. S. Thakur⁴

¹ *Indian Institute of Astrophysics, Block II, Koramangala, Bangalore 560 034, India*

² *Departamento de Astronomia, Universidad de Guanajuato, Guanajuato, CP36000, Mexico*

³ *Laboratoire d'Astrophysique, Ecole Polytechnique Fédérale de Lausanne (EPFL), Observatoire de Sauverny, CH-1290, Versoix, Switzerland*

⁴ *Behind BSF Complex, Paloura Top, Jammu - 181124, India*

Accepted ... Received ...; in original form ...

ABSTRACT

We present the results of our optical monitoring campaign of the X-ray source H 0507+164, a low luminosity Seyfert 1.5 galaxy at a redshift, $z = 0.018$. Spectroscopic observations were carried out during 22 nights in 2007, from the 21 of November to the 26 of December. Photometric observations in the R-band for 13 nights were also obtained during the same period. The continuum and broad line fluxes of the galaxy were found to vary during our monitoring period. The R-band differential light curve with respect to a companion star also shows a similar variability. Using cross correlation analysis, we estimated a time delay of $\tau_{cen} = 3.01^{+0.42}_{-1.84}$ days (in the rest frame), of the response of the broad H_β line fluxes to the variations in the optical continuum at 5100 Å. Using this time delay and the width of the H_β line, we estimated the radius for the Broad Line Region (BLR) of $2.53^{+0.35}_{-1.55} \times 10^{-3}$ parsec, and a black hole mass of $9.62^{+0.33}_{-3.73} \times 10^6 M_\odot$.

Key words: galaxies:active - galaxies:individual (H 0507+164) - galaxies:Seyfert

1 INTRODUCTION

Accretion of gas onto a Super Massive Black Hole (SMBH) in the nucleus of galaxies is believed to be the source of activity in Quasars and Seyfert galaxies (commonly known as Active Galactic Nuclei (AGNs); cf. Rees 1984). Several studies have suggested that the mass of the SMBH in these objects is correlated with the luminosity, mass and velocity dispersion of the stellar spheroid of the galaxies (Kormendy & Richstone 1995; Magorrian et al. 1998; Ferrarese & Merritt 2000; Gebhardt et al. 2000; Marconi & Hunt 2003; Häring & Rix 2004). Such correlations may imply an evolutionary relation between the growth of the SMBH and the host galaxy itself (e.g. Somerville et al. 2008; Shankar et al. 2009; Hopkins & Hernquist 2009). In order to study the dependence of the various observed phenomena of AGNs on the black hole mass and the cosmic evolution of the black holes, independent and reliable estimates of the mass of the black holes are required (e.g., Goulding et al. 2010; Rafter, Crenshaw & Wiita 2009).

One independent method to estimate the mass of the black hole is using the reverberation mapping technique

(Blandford & McKee 1982; Peterson 1993). In the optical bands, the continuum flux of some AGNs, is known to vary on timescales as short as hours (e.g., Miller, Carini & Goodrich 1989; Stalin et al. 2004). If the main source of ionization of the Broad Line Region (BLR) is the continuum itself, any variation of the continuum emission can also be seen in the broad emission lines. However, the variations in the broad line flux will have a time lag (τ) relative to the continuum variations, which can be interpreted as the light travel time across the BLR. As a first approximation, therefore, the size of the BLR is $R_{BLR} \leq c\tau$, where c is the velocity of light. Once the R_{BLR} is obtained, the mass of the black hole can also be estimated, using the velocity dispersion of the broad component of the emission lines, σ_{line} , and assuming virial equilibrium (Peterson et al. 2004; P04; see Peterson 2010, for a recent review).

The reverberation mapping technique has been used to make estimates of SMBH masses over a large range of redshift. However, because the technique is observationally taxing, as it demands an enormous amount of telescope time, to date the BLR radius of only about three dozen AGNs (Seyfert 1 galaxies and Quasars) have been determined (P04; Kaspi et al. 2007; Bentz et al. 2009a; Denney et al. 2009, 2010). Nevertheless, using these estimates a correlation was

* E-mail: stalin@iiaa.res.in

found between R_{BLR} and the optical continuum luminosity at 5100 Å (Kaspi et al. 2000; Kaspi et al. 2007; P04; Denney et al. 2009; Bentz et al. 2009b). The $R_{BLR}-\lambda L_{5100\text{Å}}$ relation can be considered well constrained between the luminosities $10^{43} \text{ erg sec}^{-1} < \lambda L_{5100\text{Å}} < 10^{45} \text{ erg sec}^{-1}$. On the other hand, for luminosities below $10^{43} \text{ erg sec}^{-1}$, only a handful of sources are observed, and the estimated values of R_{BLR} could also indicate a flattening of the relation (see Fig. 2 of Kaspi et al. 2005). This flattening would suggest a lower limit in the possible masses of SMBHs in galaxies. Although recent revisions of a few sources made by Bentz et al. (2006) and Denney et al. (2009;2010) are consistent with a continuation of the $R_{BLR}-\lambda L_{5100\text{Å}}$ relation to lower luminosities, and consequently with no lower limit in the mass for the SMBH, the correlation is still sparsely sampled. Moreover, the $R_{BLR}-\lambda L_{5100\text{Å}}$ relation is very useful for estimating the SMBH masses from single-epoch spectra and calibrating other surrogate relations used for black hole mass estimates (Vestergaard 2004; Shen et al. 2008). Therefore, estimates of R_{BLR} for a larger number of sources are required.

The extrapolation of the known $R_{BLR}-\lambda L_{5100\text{Å}}$ relation to low luminosities suggests that the time lag between the variations of the broad line and that of the continuum will be of the order of hours to days, as compared to several months for high luminosity sources. Thus, monitoring programs of short durations, but fast sampling, are required to estimate the reverberation time lags for low luminosity sources.

In this paper, we present the optical spectroscopic and photometric observations of a new low luminosity AGN, the X-ray source and Seyfert 1.5 galaxy H 0507+164. Based on a reverberation mapping campaign that lasted for about a month, during November-December 2007, we have obtained R_{BLR} and estimated the mass of the SMBH. In Section 2, the observations and data reductions are described. The results of the analysis are given in Section 3, and the conclusions are presented in Section 4.

2 OBSERVATIONS AND REDUCTIONS

Using the Véron-Cetty & Véron catalogue of Quasars and Active Galactic Nuclei (12th Ed.; Véron-Cetty & Véron 2006), we have compiled a list of nearby Seyfert 1 galaxies, which, based on the available spectra, have a luminosity at $\lambda 5100$ Å of the order of $10^{42} \text{ erg sec}^{-1}$ or lower. Very few candidates were found (mostly because of the absence of available spectra). The source, H 0507+164, that we selected for our campaign is identified in the catalogue of Véron-Cetty & Véron as an X-ray source, with coordinates $\alpha_{2000} = 05^h 10^m 45.5^s$, $\delta_{2000} = 16^d 29^m 56^s$, and is classified as a Seyfert 1.5 galaxy at a redshift of $z = 0.018$.

Optical spectroscopic and photometric observations of H 0507+164 were carried out in 2007 between 21 of November and 26 of December at the 2m Himalayan Chandra Telescope (HCT), operated by the Indian Institute of Astrophysics, Bangalore. The telescope is equipped with a 2048×4096 CCD, coupled to the Himalayan Faint Object

Spectrograph and Camera (HFOSC)¹. In imaging mode, only the central 2048×2048 pixels region of the CCD is used. The camera has a plate scale of 0.296 arcsecond/pixel, which yields a field of view of 10×10 square arcmin.

2.1 Spectroscopy

Medium resolution spectra of the nucleus were obtained using a $11 \text{ arcmin} \times 1.92 \text{ arcsec}$ wide slit and a grism. The spectra have a spectral range of 3800–6700 Å with a resolution of ~ 8 Å. The exposure time varied between 900 and 1000 seconds. The spectra were reduced using standard procedures in IRAF². After bias subtraction and flat fielding, one dimensional spectra were extracted and calibrated, in wavelength using an FeAr lamp, and in flux using various observations of the spectrophotometric standard star Feige 34. Since the observed spectra were of low S/N, for further analysis all the spectra were smoothed to a resolution of ~ 15 Å.

The standard technique of spectral flux calibration is not sufficiently precise to study the variability of AGNs. Since even under good photometric conditions the accuracy of spectrophotometry is not better than 10% (Shapovalova et al. 2008), we used a relative calibration procedure. A first order flux calibration was first obtained in the normal way using the standard star. Then all the spectra were intercalibrated relative to the spectra of one night (we choose the 21 of November), assuming the flux of the narrow line [O III] $\lambda 5007$ Å is constant. This is justified, because the Narrow Line Region (NLR) is much more extended (of the order of a few hundred parsecs) than the BLR (much less than a parsec) and flux variation cannot be observed in this region over short time scales (cf. Osterbrock 1989). Each spectra were scaled relative to the reference spectra using the scaling algorithm devised by van Groningen & Wanders (1992). This algorithm uses a chi-square, to minimize the residuals of the [O III] $\lambda 5007$ Å line after subtraction from the reference spectrum. The mean spectrum, averaging the 22 nights of observations, is shown in Fig. 1.

2.2 Photometry

In parallel to the spectroscopic observations, R-band images were also obtained with the HFOSC. Unfortunately, some observations turned out to be contaminated by the light of the extremely bright stars located near the source. As a consequence, our R-band photometry covers only 13 of the 22 nights of the campaign. The images were bias subtracted and flat fielded using IRAF packages. For the rest of the reduction, calibration and analysis, packages in MIDAS³ were used. After removing the cosmic rays, profile fitting photometry was done using the DAOPHOT and ALLSTAR packages. The observed R-band frame is shown in Fig. 2.

¹ http://www.iap.res.in/iao_hfosc

² IRAF stands for Image Reduction and Analysis Facility and is distributed by the National Optical Astronomy Observatories, which is operated by the Association of Universities for Research in Astronomy, Inc. under contract to the National Science Foundation

³ Munich Image Data Analysis System; trademark of the European Southern Observatory

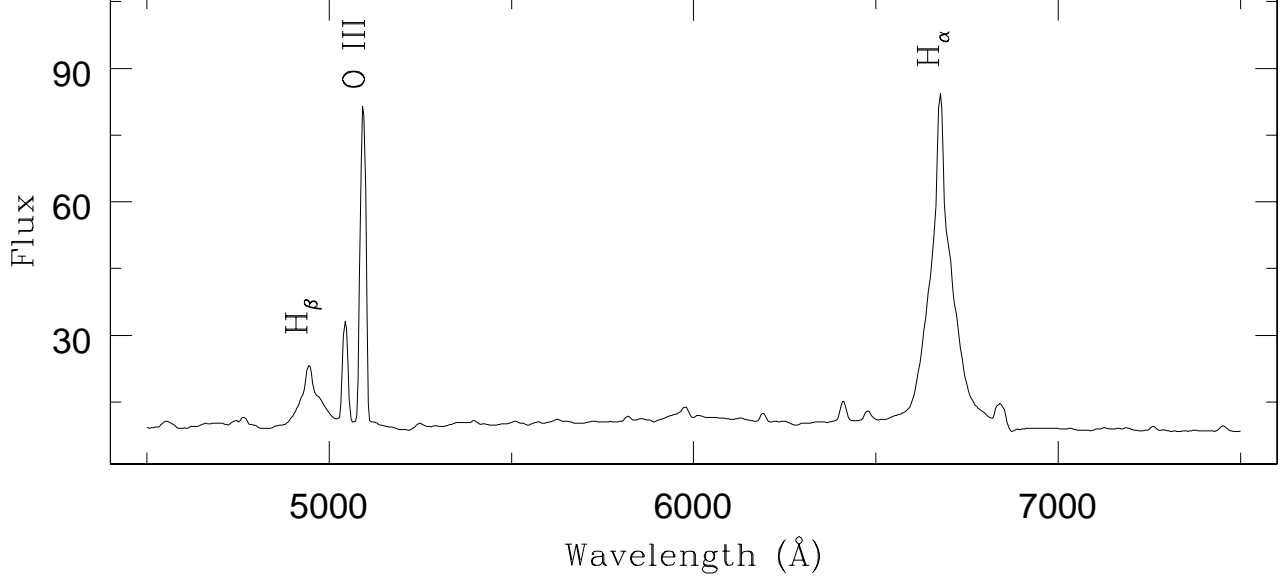


Figure 1. Average spectrum of H 0507+164 obtained by averaging the observations of the 22 nights. The flux is in the unit of $10^{-16} \text{ erg cm}^{-2} \text{ s}^{-1} \text{ Å}^{-1}$. The classification as Seyfert 1.5 is confirmed, as one can see both a broad and narrow component for the $\text{H}\beta$ line at $\lambda 4861 \text{ Å}$ (cf. Osterbrock 1989).

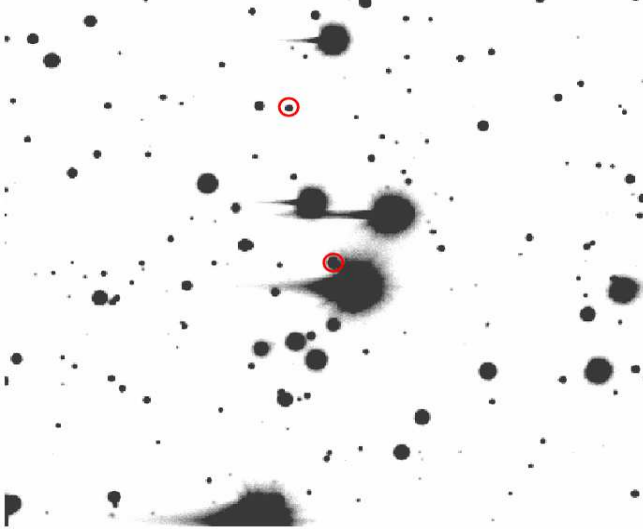


Figure 2. The R-band image of H 0507+164. The galaxy (in the center) and comparison star (on the top) used for differential photometry are indicated by circles. The field of view has a dimension of 10×10 arcmin. North is up and east is to the left. Note the presence of an extremely bright star near H 0507+164.

3 ANALYSIS

3.1 Lightcurves

The lightcurves of the $\text{H}\beta$ flux and the continuum at 5100 Å were obtained using the final inter-calibrated spectra. The continuum flux in the rest-frame of the galaxy at 5100 Å was obtained using the mean flux within the observed band from 5172 to 5200 Å .

The $\text{H}\beta$ emission line fluxes were obtained by integrat-

Table 1. Continuum and $\text{H}\beta$ fluxes for the source H 0507+164

Julian Date	$F_{\lambda} \times 10^{-16}$ 5100 Å (erg/s/cm ² /Å)	$H_{\beta} \times 10^{-14}$ 4861 Å (erg/s/cm ² /Å)	Δm (mag)
-2454420			
6.434	6.30 ± 0.07	5.07 ± 0.05	-0.022 ± 0.012
7.289	7.19 ± 0.10	5.62 ± 0.07	0.020 ± 0.015
13.429	7.04 ± 0.11	5.14 ± 0.07	
14.389	7.59 ± 0.07	5.56 ± 0.05	
15.375	7.98 ± 0.09	5.11 ± 0.06	-0.274 ± 0.009
16.281	8.08 ± 0.06	5.37 ± 0.05	-0.285 ± 0.008
17.376	8.35 ± 0.08	5.64 ± 0.05	
18.391	8.22 ± 0.07	5.47 ± 0.05	-0.206 ± 0.010
19.442	8.51 ± 0.09	5.52 ± 0.06	-0.313 ± 0.007
20.391	8.26 ± 0.07	5.78 ± 0.05	
21.421	8.39 ± 0.09	5.90 ± 0.07	-0.364 ± 0.010
29.423	9.88 ± 0.10	6.41 ± 0.07	
30.366	9.90 ± 0.08	6.38 ± 0.06	-0.343 ± 0.009
31.416	9.86 ± 0.13	5.51 ± 0.09	-0.515 ± 0.006
34.183	9.83 ± 0.09	6.13 ± 0.06	-0.422 ± 0.009
35.257	10.13 ± 0.37	7.78 ± 0.24	-0.437 ± 0.018
36.185	10.30 ± 0.15	6.62 ± 0.10	
37.146	10.33 ± 0.23	7.54 ± 0.14	
38.092	8.57 ± 0.42	8.90 ± 0.26	
39.075	11.96 ± 0.36	9.23 ± 0.22	
40.167	11.53 ± 0.15	7.64 ± 0.10	-0.554 ± 0.007
41.326	10.40 ± 0.13	6.69 ± 0.08	-0.536 ± 0.008

ing the emission profile in the band spanning $4884\text{--}5012 \text{ Å}$, after subtracting a continuum. An average of the mean fluxes in the regions on the blue ($4808\text{--}4852 \text{ Å}$) and red ($5012\text{--}5024 \text{ Å}$) sides of the $\text{H}\beta$ line was used as the continuum below the line. Although the measured line fluxes include both the narrow and broad components, any variation observed in the line fluxes can be attributed to the

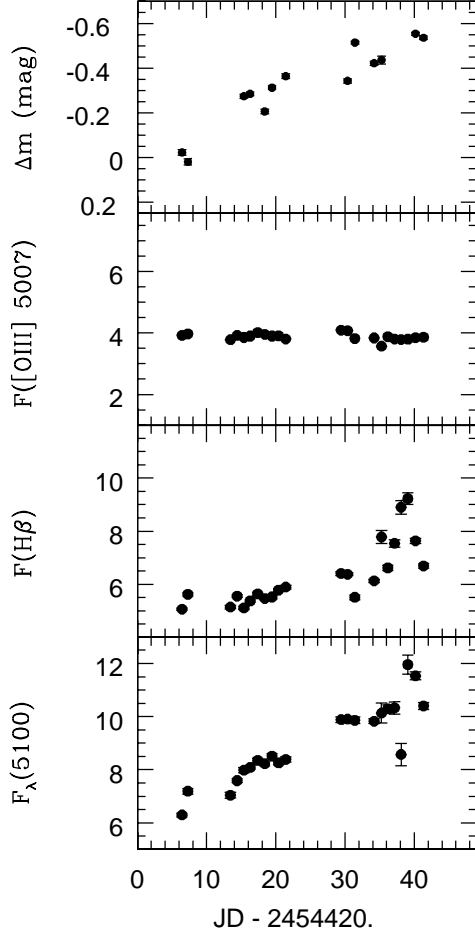


Figure 3. The R-band differential lightcurve (top panel), followed by the lightcurves for [O III] $\lambda 5007$ Å, H_{β} and continuum at 5100 Å are plotted. The fluxes are in units of 10^{-13} erg s $^{-1}$ cm $^{-2}$ Å $^{-1}$ for the [O III] $\lambda 5007$ Å line, 10^{-14} erg s $^{-1}$ cm $^{-2}$ Å $^{-1}$ for the H_{β} line and 10^{-16} erg s $^{-1}$ cm $^{-2}$ Å $^{-1}$ for the continuum.

broad component only, since the narrow component is not expected to vary during the period of our observations. The lightcurves for the continuum at 5100 Å, for the H_{β} and for the [O III] $\lambda 5007$ Å lines are shown in Fig. 3. The corresponding fluxes for the continuum and H_{β} are listed in Table 1. As expected from the inter-calibration procedure, the lightcurve for [O III] $\lambda 5007$ Å is nearly constant. On the other hand, both the continuum at 5100 Å and the H_{β} flux are observed to vary.

The observed R-band differential instrumental magnitudes between the galaxy and the comparison star (marked in Fig. 3) are also given in Table 1. The R-band differential lightcurve plotted in Fig. 3 (top panel) closely follows the lightcurves of the continuum at 5100 Å and H_{β} . The average flux at 5100 Å is $9.03 \pm 1.47 \times 10^{-16}$ erg cm $^{-2}$ s $^{-1}$ Å $^{-1}$, which corresponds to $\lambda L_{5100\text{Å}}$ of $3.4 \pm 0.55 \times 10^{42}$ erg s $^{-1}$, for the cosmological parameters $H_0 = 70$ km s $^{-1}$ Mpc $^{-1}$, $\Omega_m = 0.3$ and $\Omega_{\Lambda} = 0.7$.

The variability of the light curves are characterised by the parameters, excess variance, F_{var} and the ratio between the maximum and minimum flux of the light curves, R_{max} (Rodriguez-Pascual et al. 1997; Edelson et al. 2002). The continuum and H_{β} line have F_{var} of 0.16 and 0.18 and R_{max} of 1.9 ± 0.020 and 1.8 ± 0.016 respectively. These values are within the range of values found by other variability studies of AGNs (cf. P04; Denney et al. 2010).

3.2 Time Lag

The time lag between the variations of the continuum flux and the variations of the H_{β} emission can be determined by cross-correlating the two light curves. For cross correlation analysis, the method of interpolated cross-correlation function (ICCF; Gaskell & Sparke 1986; Gaskell & Peterson 1987) and the method of discrete correlation function (DCF; Edelson & Korlik 1998) were used. Although both ICCF and DCF methods produce similar results (White & Peterson 1994), the interpolation of the light curve during the period of gaps required by the ICCF method might not be a reasonable approximation to the behavior of the light curves. Thus the DCF method is preferable for data with large gaps (Denney et al. 2009). For comparison, we obtain the results using both the methods.

The results of the cross correlation analysis are shown in Fig. 4. The cross correlation function (CCF) obtained using the ICCF method is plotted as a thick solid line. The auto correlation functions (ACFs) of the continuum at 5100 Å and the H_{β} line are also shown in Fig. 4 as dashed and dotted lines respectively. For comparison the cross correlation function obtained using the DCF method is also plotted as a thin solid line. As expected, the auto correlations have zero time lags. On the other hand, the time lag in the cross correlation curve is clearly noticeable as an overall shift to the right. The position of the maximum in the CCF provides an estimate of the time lag between the continuum and the H_{β} line. The maximum was however determined using the centroid, which gives a better estimate for noisy CCFs, rather than the peak, using the formula:

$$\tau_{cen} = \frac{\sum_i \tau_i CCF_i}{\sum_i CCF_i} \quad (1)$$

The estimate of the centroid includes all the points that are within 50% of the peak value of the CCF. Based on this cross correlation analysis, a statistically significant centroid and the associated uncertainty were obtained using a bootstrap technique that introduces effects of randomness in fluxes and sampling of the light curve (cf. P04). A method to carry out Monte-Carlo (MC) simulation using the combined effects of flux randomization (FR) and the random subset selection (RSS) procedures is described in Peterson et al. (1998). Additional improvements as suggested by Welsh (1999) are summarised in P04, which we use for our analysis.

First an RSS procedure was applied by randomly selecting 22 observations from the light curve. The flux uncertainties of the multiply selected observations were weighted according to Welsh (1999). This light curve was given as input to the FR procedure, where each measured value of the fluxes are modified by adding the measured flux uncertainties multiplied with a random Gaussian value. The

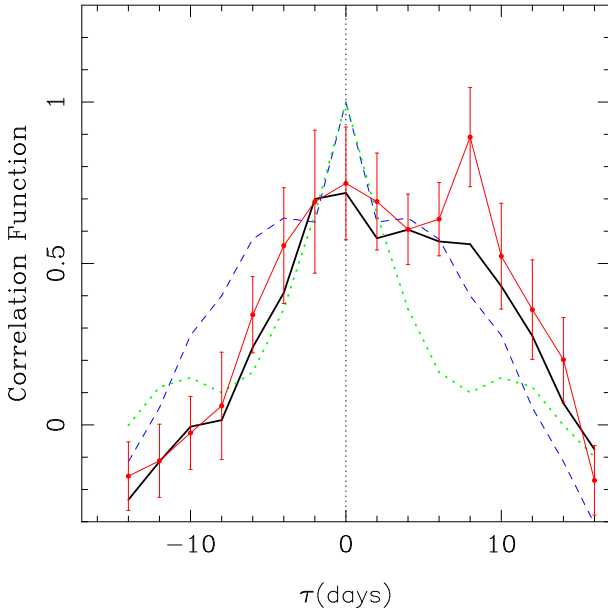


Figure 4. The cross correlation function of the continuum at 5100 Å and the $H\beta$ lightcurves, as obtained using the ICCF method, is plotted as a thick solid line. The auto correlation functions of the continuum at 5100 Å and the $H\beta$ line are plotted as dashed and dotted lines respectively. The cross correlation function obtained using the DCF method is plotted as a thin solid line.

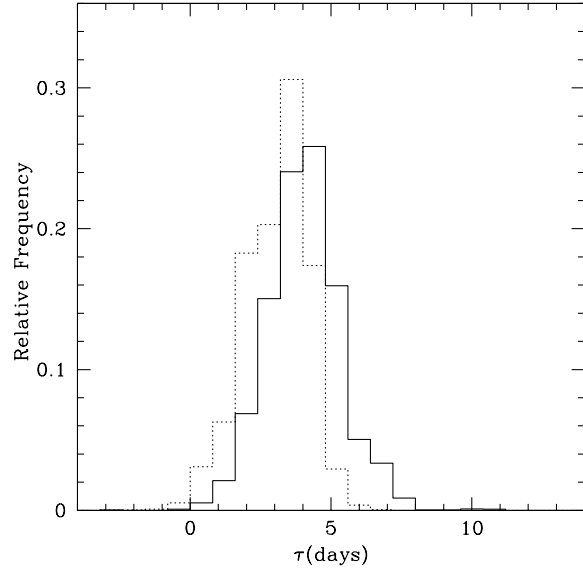


Figure 5. Histogram of the cross-correlation centroids obtained using the FR/RSS realisations. The solid and dotted lines represent the cross-correlation centroid distributions (CCCDs) determined using the ICCF and DCF respectively, for a bin size of 2 days.

Table 2. Estimates of centroid values obtained using the DCF and ICCF methods.

Method	Size of the bin (days)				
	2	2.5	3	3.5	4
ICCF	$3.14^{+0.95}_{-1.08}$	$3.28^{+0.67}_{-1.60}$	$3.27^{+0.66}_{-1.64}$	$3.06^{+0.43}_{-1.87}$	$3.05^{+0.40}_{-1.74}$
DCF	$3.91^{+1.30}_{-1.07}$	$4.30^{+1.46}_{-1.44}$	$4.19^{+1.77}_{-0.86}$	$4.11^{+1.19}_{-1.49}$	$4.03^{+0.94}_{-1.40}$

modified light curves were then cross-correlated and the centroids were determined as outlined above using CCF values above 50% of the peak value. This procedure was repeated for 4000 times, retaining only those CCFs whose maximum cross-correlation coefficient is large enough such that the correlation is significant with a confidence level of 95% or larger. A cross-correlation centroid distribution (CCCD) was built using the above centroids and is shown in Fig. 5. The average value of CCCD was taken to be τ_{cent} . Since the CCCD is non-Gaussian (cf. Peterson et al. 1998), the upper and lower uncertainties in τ_{cent} were determined such that 15.87% of CCCD realizations have $\tau > \tau_{cent} + \Delta\tau_{up}$ and 15.87% realizations have $\tau < \tau_{cent} - \Delta\tau_{low}$. This error in τ_{cent} corresponds to $\pm 1\sigma$ errors for a Gaussian distribution.

The centroid time lags obtained using different cross correlation methods for different bin sizes are given in Table 2. The variations due to different bin sizes are within the error bars. The DCF method gives a mean time lag of about 4 days, whereas the ICCF method gives a mean value of about 3 days. This difference is of the order of the estimated errors on the time lags. Considering these uncertainties, both the DCF and ICCF methods give time delays that are consistent with each other. This suggests that the

estimated time lag is not a spurious result for the sampling of the light curves presented here, and the results of the ICCF methods are reliable. To be conservative, for further calculations we use the time lag with the largest scatter corresponding to a bin size of 3.5 days, obtained using the ICCF method.

Based on this analysis the average observed frame time lag between the $H\beta$ and the $\lambda 5100$ Å continuum light-curves was found to be $3.06^{+0.43}_{-1.87}$ days. After correcting for the time dilation effects using the redshift of the source, we found a time lag of $3.01^{+0.42}_{-1.84}$ days in the rest frame of the source.

The wavelength coverage of our observations, also include the $H\alpha$ line, and a time lag using the $H\alpha$ line can also be estimated. However, by repeating the analysis procedure presented here, a reliable time lag using $H\alpha$ line could not be found, because the correlation curves are too noisy. This may be due to the shorter duration of the observations and the relative flux calibration procedure using the [O III] $\lambda 5007$ Å line situated much farther apart in wavelength from $H\alpha$ being unreliable (Grier et al. 2008). Unfortunately, the nearby doublet [S II] $\lambda\lambda 6716, 6731$ Å narrow lines, which could be used for the relative calibration of $H\alpha$, are too weak. Thus we do not estimate the time lag using the $H\alpha$ line.

3.3 Line width

In order to relate the time lag to the mass of the black hole, an estimate of the line width, the line dispersion σ_{line} , of the broad emission component of $H\beta$, is required. Following P04, it is relatively straight forward and more practical to measure σ_{line} , the second moment of the profile, directly from the root mean square (rms) spectrum. Indeed, in the rms spectrum the constant components, or those that vary on timescales much longer than the duration of the observation

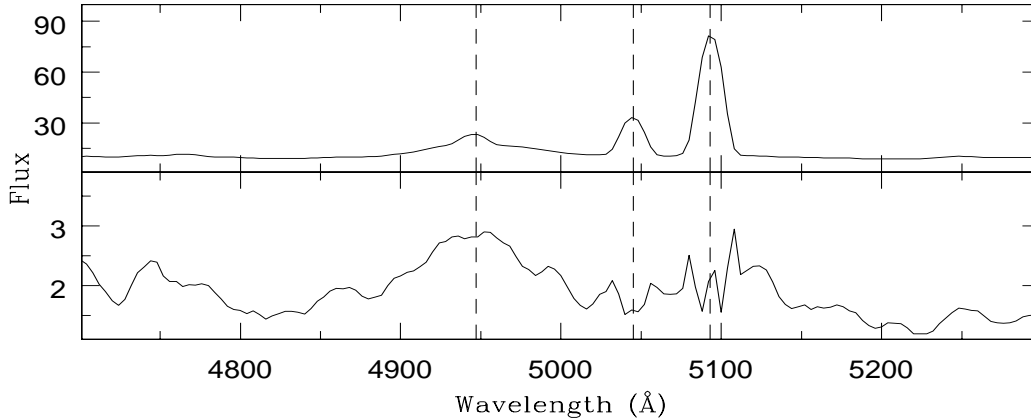


Figure 6. A zoomed up version of the mean spectrum (top panel) and corresponding rms spectrum (bottom panel). The flux is in the unit of $10^{-16} \text{ erg cm}^{-2} \text{ s}^{-1} \text{ Å}^{-1}$. The rms spectrum shows negligible contribution from the two [O III] narrow lines.

vanish, thus largely obviating the problem of de-blending the lines. To obtain the rms spectrum, all the observed spectra were combined using the formula:

$$S(\lambda) = \left\{ \frac{1}{N-1} \sum_{i=1}^N [F_i(\lambda) - \bar{F}(\lambda)]^2 \right\}^{\frac{1}{2}} \quad (2)$$

In Fig. 6, we show the root mean square (rms) spectrum. It can be seen that the two narrow [O III] lines have almost completely disappeared in the rms spectrum.

The mean value of σ_{line} corrected for the instrumental response of the spectrograph and the associated uncertainty were obtained following the bootstrap method described in P04. From our observed 22 observed spectra, we randomly selected 22 spectra, irrespective of whether a particular spectrum has already been selected or not. Since some of the spectra were selected multiple times, the mean value of the resultant number of spectra were smaller by 8. These randomly selected spectra were then used to construct an rms spectra from which σ_{line} was measured and corrected for the instrumental resolution of the spectrograph. This procedure was repeated 10000 times and the mean and standard deviation of these realisations are taken as σ_{line} and its uncertainty respectively. A distribution of σ_{line} values obtained from the bootstrap method is also shown in Fig 7. We thus estimate a line dispersion of $\sigma_{line} = 1725 \pm 105 \text{ km sec}^{-1}$.

3.4 R_{BLR} and the mass of the black hole

Using the rest frame time delay, the radius of the BLR is estimated to be $R_{BLR} = 2.53^{+0.35}_{-1.55} \times 10^{-3} \text{ pc}$. In Fig. 8 we show the measurement of R_{BLR} and $\lambda L_{5100\text{Å}}$ luminosity of the source presented here along with the most updated data set given by Bentz et al. (2009b) and the additional source, Mrk 290, given by Denney et al. (2010). The solid line is the relation obtained by Bentz et al. (2009b). From this figure it can be seen that our H_{β} measurement lags are in agreement with the known $R_{BLR} - L$ relationship.

The mass of the black hole was estimated using the formula in P04:

$$M_{BH} = f \frac{R_{BLR} \Delta V^2}{G} \quad (3)$$

where ΔV is the width of the line and G is the gravitational constant. The parameter f is a scaling factor, which takes into account the geometry and kinematics of the BLR. Onken et al. (2004) found an empirical value of $f = 5.5$, using a sample of AGNs having both reverberation based black hole masses and host galaxy bulge velocity dispersion (σ_*) estimates. This value relies on the assumption that both AGNs and quiescent galaxies follow the same $M_{BH} - \sigma_*$ relationship (Ferrarese & Merritt 2000; Gebhardt et al. 2000). For this particular scaling, the appropriate velocity width ΔV is the line dispersion in the rms spectrum σ_{line} (Bentz et al. 2008). Adopting the Onken et al. (2004) scaling factor and the σ_{line} measured from our observations, we estimated the mass of the SMBH in H 0507+164 to be $M_{BH} = 9.62^{+0.33}_{-3.73} \times 10^6 M_{\odot}$.

4 CONCLUSION

We present for the first time monitoring observations of the X-ray source and Sy 1.5 galaxy H 0507+164, spanning a time period of about one month. We have obtained 22 nights of spectra during this period, with a mean sampling time of about 1.6 days. We measured an observed frame time lag of about $3.06^{+0.43}_{-1.87}$ days between the changes in the H_{β} emission line flux and the changes in the continuum flux at 5100 Å. After correcting for the redshift, we find a corresponding time lag of $3.01^{+0.42}_{-1.84}$ days in the rest frame of the source. From this measured time lag we deduced a size for the BLR of $R_{BLR} = 2.53^{+0.35}_{-1.55} \times 10^{-3}$ parsec and estimated a black hole mass of $9.62^{+0.33}_{-3.73} \times 10^6 M_{\odot}$. Our estimate of R_{BLR} using the measured lag of H_{β} is in agreement with the $R_{BLR} - \lambda L_{5100\text{Å}}$ relationship shown by Bentz et al. (2009b).

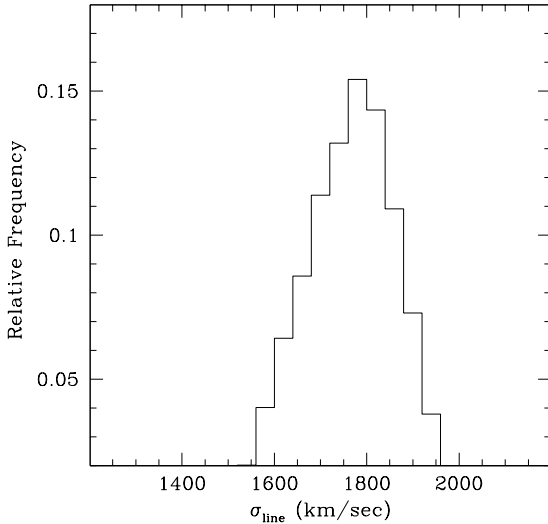


Figure 7. Histogram of the estimates of the σ_{line} using the bootstrap method described in the text.

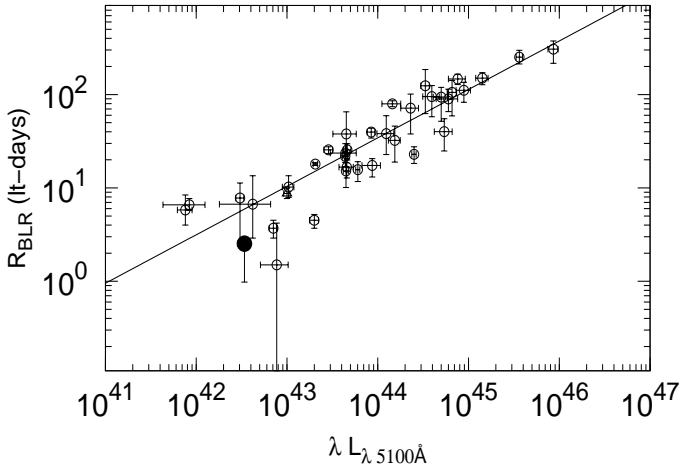


Figure 8. The radius of the BLR vs the continuum luminosity at 5100 Å. The open circles are from Bentz et al. (2009b). The open triangle is the source Mrk 290 reported by Denney et al. 2010. The solid line (with a slope of 0.519) is the fit obtained by Bentz et al. (2009b). The new measurement of this work is shown as a filled circle.

ACKNOWLEDGMENTS

We thank the anonymous referee for his/her valuable comments that helped to improve the presentation significantly. We also thank B. M. Peterson and R. W. Pogge for kindly providing us with the relative flux scaling program. The support provided by the staff at the Indian Astronomical Observatory, Hanle and CREST, Hoskote is also acknowledged.

REFERENCES

- Bentz M.C. et al. 2006, ApJ, 651, 775
 Bentz M.C. et al. 2008, ApJ, 689, L21
 Bentz M.C. et al. 2009a, ApJ, 705, 199
 Bentz M.C. et al. 2009b, ApJ, 697, 160
 Blandford R. D., McKee, C. F. 1982, ApJ, 255, 419
 Denney K. D. et al. 2009, ApJ, 702, 1353
 Denney K. D. et al. 2010, ApJ, 721, 715
 Edelson R.A., Krolik J.H. 1988, ApJ, 333, 646
 Edelson R., Turner T. J., Pounds K., Vaughan S., Markowitz A., Marshall, H., Dobbie P., & Warwick, R. 2002, ApJ, 568, 610
 Ferrarese L., Merritt D. 2000, ApJ, 539, L9
 Gaskell C. M., Sparke L. S., 1986, ApJ, 305, 175
 Gaskell C. M., Peterson B.M., 1987, ApJS, 65, 1
 Gebhardt K. et al. 2000, ApJ, 539, L13
 Goulding A. D., Alexander D. M., Lehmer B. D., Mullaney J. R. 2010, MNRAS, 406, 597
 Grier C. J., et al. 2008, ApJ, 688, 837
 Häring N., Rix H.-W. 2004, ApJ, 604, L89
 Hopkins P. F., Hernquist L. 2009, ApJ, 694, 599
 Kaspi S., Smith P.S., Netzer H., Maoz D., Jannuzi B.T., Givon U. 2000, ApJ, 533, 631
 Kaspi S., Maoz D., Netzer H., Peterson B.M., Vestergaard M., Jannuzi B.T. 2005, ApJ, 629, 61
 Kaspi S., Brandt W. N., Maoz D., Netzer H., Schneider D. P., Shemmer O. 2007, ApJ, 659, 997
 Kormendy J., Richstone D. 1995, ARA&A, 33, 581
 Magorrian J. et al. 1998, AJ, 115, 2285
 Marconi A., Hunt L. K. 2003, ApJ, 589, L21
 Miller H.R., Carini M.T., Goodrich B.D. 1989, Nature, 337, 627
 Onken C.A., Ferrarese L., Merritt D., Peterson B.M., Pogge R.W., Vestergaard M., Wandel A. 2004, ApJ, 615, 645
 Osterbrock D. E 1989, in Astrophysics of Gaseous Nebulae and Active Galactic Nuclei, University Science Book
 Peterson B. M., Wanders I., Horne K., Collier S., Alexander T., Kaspi S., Maoz D., 1998, PASP, 110, 660
 Peterson B. M. 1993, PASP, 105, 247
 Peterson B. M., et al. 2004, ApJ, 613, 682
 Peterson B.M., 2010, IAU Symposium, 267, 151
 Rafter S. E., Crenshaw D. M., Wiita P. J. 2009, AJ, 137, 42
 Rees M. J. 1984, ARA&A, 22, 471
 Rodriguez-Pascual P. M., et al. 1997, ApJS, 110, 9
 Shankar, F., Weinberg, D. H., Miralda Escudé, J. 2009, ApJ, 690, 20
 Shapovalova A.I. et al. 2008, A&A, 486, 99
 Shen Y., Greene J.E., Strauss M.A., Richards G.T., Schneider D. P. 2008, ApJ, 680, 169
 Somerville R. S., Hopkins P. F., Cox T. J., Robertson B. E., Hernquist L. 2008, MNRAS, 391, 481
 Stalín C.S., Gopal-Krishna, Sagar R., Witta P.J. 2004, JApA, 25, 1
 van Groningen E., Wanders I. 1992, PASP, 104, 700
 Véron-Cetty M.P., Véron P. 2006, A&A, 455, 776
 Vestergaard M. 2004, ApJ, 601, 676
 Welsh W. F., 1999, PASP, 111, 1347
 White R. J., Peterson B. M., 1994, PASP, 106, 879